

# BIRD AND DRONE IMPACT DAMAGE PROGNOSIS OF ON-DEMAND AIR MOBILITY SERVICE AIRCRAFT ENGINE

Hasan Raza<sup>1</sup>, Pradeep Vaghela<sup>1</sup> Eike Stumpf<sup>2</sup>, and Javid Bayandor<sup>1</sup>

<sup>1</sup>CRashworthiness for Aerospace Structures and Hybrids (CRASH) Lab
Department of Mechanical and Aerospace Engineering
University at Buffalo - The State University at New York, NY, 14260, USA
<sup>2</sup>Institute for Aerospace Systems, RWTH AACHEN University, 52062 Aachen, Germany

#### **Abstract**

The development of advanced on-demand air mobility services, also referred to as air taxis, is on the rise to help divert pressure from existing transportation modes. Due to more frequent take offs and landings, air taxis' close encounter with birds and drones drastically increases within the latter's flight or operating altitudes. In this study, finite element methods and analysis are used to investigate damage due to direct and oblique impact from a bird and drone on the engine of a modern air taxi following existing certification standards. A bird surrogate modeled using the Smoothed Particle Hydrodynamics (SPH) method, and a quadcopter drone were used as projectiles. Results from the impacts are analyzed and compared to investigate the post-impact damage of the aircraft engine.

Keywords: Air Taxi, Bird-strike, Drone Impact, Engine Ingestion, Finite Element Analysis

## 1. Introduction

Traditional transportation modes are reaching their infrastructure and capacity limits, yet the demand for transportation is ever-growing due to the rapid progress in globalization. Advanced air mobility (AAM), also referred to as on-demand air mobility (ODAM) services [1-3], are on the rise due to their potential for addressing shortcomings related to current transportation systems. Traditionally, the aviation industry's focus has been on enabling long-distance travel, which is why aircraft typically fly at higher altitudes. However, with the increasing interest and demand for ODAM services, many companies are in the process of developing flight solutions that can make short-distance air travel possible; one such company is e.SAT GmbH's Silent Air Taxi [4], a piloted four-passenger aircraft. Any air transportation system is prone to foreign object impact (FOI) such as bird-strikes during takeoff and landing. ODAM aircraft make more frequent stops in regional areas, and therefore need to fly at relatively lower altitudes, making them more susceptible to bird-strikes, as depicted in Fig. 1. Wildlife-strikes, which primarily include birds, terrestrial mammals and reptiles, were reported to be around 241,000 [5], from over 2,000 U.S. airports from 1991 to 2021. The number of strikes reported to the FAA increased from 1,850 in 1990 to a record high of 17,228 in 2019, a 9.3-fold increase. In 2019, birds were involved in 94% of the reported strikes. The annual cost of wildlife-strikes was projected to be 116,984 hours of aircraft downtime and \$205 million in monetary losses [5] to the U.S. civil aviation industry in 2019. The actual number of bird-strike incidents may be higher as the data only reflects the reported incidents.

The Federal Aviation Administration (FAA) has implemented guidelines and requirements to enhance aircraft safety against bird-strikes. Small aircraft such as e.SAT, as well as other ODAM fall within the purview of the FAA's 14 CFR PART 23 [7], which focuses on airworthiness standards for normal, utility and commuter category airplanes. In terms of bird impact airworthiness standards, the guidelines stipulate that for Level 4 airplanes, the canopy and its supporting structure in front of the pilot must be able to withstand the impact of a 2 lb bird at the aircraft's maximum approach flap

speed without experiencing penetration [7]. In addition to bird-strikes, collision incidents of unmanned aircraft systems (UAS) such as drones are also becoming more common. Concerns about UAS operation and safety have been ongoing [8-10], where focus has been given to developing advanced collision avoidance algorithms and systems. Damage assessment however remains a crucial aspect of reducing any catastrophic damage to civilian aircraft structures from UAS collisions. It has been shown extensively by Bayandor and the team [11-14] since 2015 that even drones within mass ranges similar to those of the certification birds for small and large piloted aircraft can pose grave collision and damage threats to their respective aircraft platform.

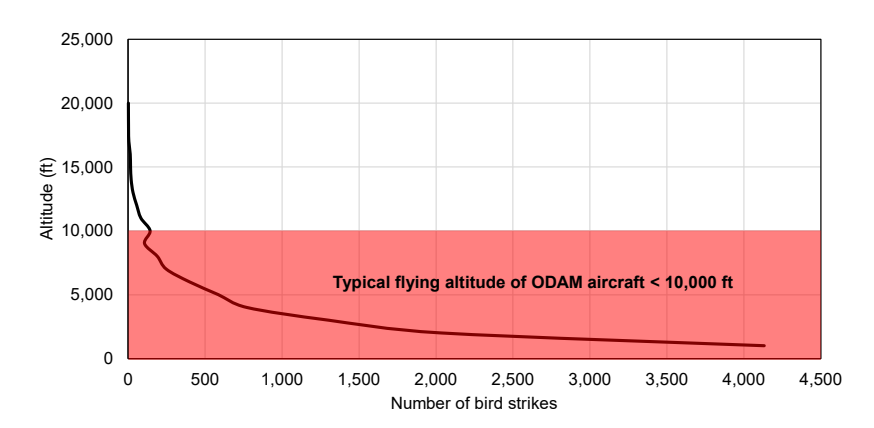


Figure 1 – Reported number of bird-strikes as a function of flying altitude of aircraft [4, 15].

Currently, no specific requirements are set to address UAV/drone impact scenarios, and there are no regulations or guidelines specifically tailored to airplanes smaller than the Level 4 category which have a maximum seating configuration of 10 to 19 passengers. It is worth noting that ODAM airplanes are typically smaller than Level 4 category aircraft. Based on statistics regarding bird-strikes [5, 6], these smaller aircraft face a similar risk as Level 4 aircraft when it comes to bird-strikes, particularly impact into the aircraft engines. The engine fan creates a large negative pressure gradient that in turn increases the chances of ingestion. Research and investigation have revealed that the jet engine has the highest chance of being subjected to foreign object impact or FOI [16, 17] among other potential impact locations on the aircraft.

There are certification guidelines that the FAA has established and developed based on extensive fuselage drop tests and bird-strike trials. However, these certification tests can only be obtained at high costs. The improvements in computational processing power fortunately have made advanced computer modeling a more reliable and cost-effective option for conducting certification studies using high-fidelity simulations [18, 19]. Based on this computational approach, analyses of FOI were considered and carried out in this study on a modern ODAM air taxi similar to eSAT. The study focused on bird impacts onto the aircraft engine. Although currently not a required certification directive, a drone impact study was also conducted, with relevant simulations performed on the engine. Fan blade damage was analyzed resulting from direct and oblique impacts by both bird and drone and compared. LS-Dyna, a commercially available explicit finite element (FE) code [20], was used due to the time-dependent nature of the impact events modeled. It should be noted that the simulated aircraft fuselage and engines in this study included the primary structural details only, and therefore it is envisaged that their impact response would be quite different to the actual full dynamic characteristics of the aircraft and engines modeled.

## 2. Computational Modeling

A commercial FE code, LS-Dyna, with several user-defined measures added by the authors, was used to perform simulations of the bird and drone impacts on a modern ODAM aircraft engine to investigate its impact and post-impact damage response. A detailed computer-aided design (CAD) model of a modern ODAM aircraft was developed for this study, shown in Fig. 2. Advanced material models and computational techniques were incorporated into the simulations to describe the damage criteria with the onset of damage and progressive failure of the engine and its components. Typical values were chosen for several parameters and variables, otherwise not available in the literature.

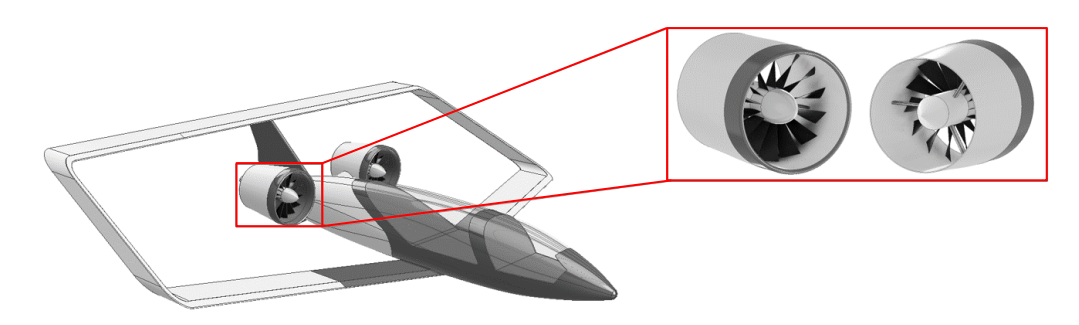


Figure 2 – CAD model of ODAM aircraft developed for this study.

# 2.1 Engine FE Model

The aircraft engines were modeled after a design representative of the engine of a small modern ODAM aircraft powered using an electric powertrain. Figure 3 shows the FE model of the engine developed for this study. The model consists of 15 Titanium (Ti-6AL-4V alloy) fan blades of 40 cm height, modeled using fully integrated solid elements. The blades were represented using the Johnson-Cook (J-C) material model. Various J-C model parameters have been referenced in the literature [21-29] for the effective modeling of Ti-6Al-4V. These parameters were obtained using different specimen sizes and strain rates. The J-C model is derived from an empirical approach that considers the large deformation, strain rate hardening, and thermal softening, as shown in Eqs. (1) through to (3).

$$\sigma = [A + B\varepsilon^n][1 + C \ln \varepsilon^*][1 - T^{*m}] \tag{1}$$

$$\varepsilon^* = \frac{\dot{\varepsilon}}{\varepsilon_o} \tag{2}$$

$$T^* = \frac{T - T_{room}}{T_{melt} - T_{room}} \tag{3}$$

where  $\sigma$  is the effective stress,  $\varepsilon$  is the effective plastic strain,  $\varepsilon^*$  is the normalized effective plastic strain rate, n is the strain hardening coefficient,  $T_{melt}$  is the melting temperature, typically taken as the solidus temperature for an alloy,  $T_{room}$  is the standard room temperature and A, B, C, and m are constants [17, 29] that are evaluated experimentally. Fracture in the J-C material model [29] is derived from the following damage law as shown in Eqs. (4) and (5).

$$D = \sum \frac{\Delta \varepsilon}{\varepsilon_f} \tag{4}$$

$$\varepsilon_f = [D_1 + D_2 \exp(D_3 \sigma^*)][1 + D_4 \ln \varepsilon^*][1 + D_5 T^*]$$
(5)

where  $\Delta \varepsilon$  is the increment of effective plastic strain during an increment in loading and  $\sigma^*$  is the mean stress normalized by the effective stress. The parameters  $D_1$ ,  $D_2$ ,  $D_3$ ,  $D_4$  and  $D_5$  are constant [29].

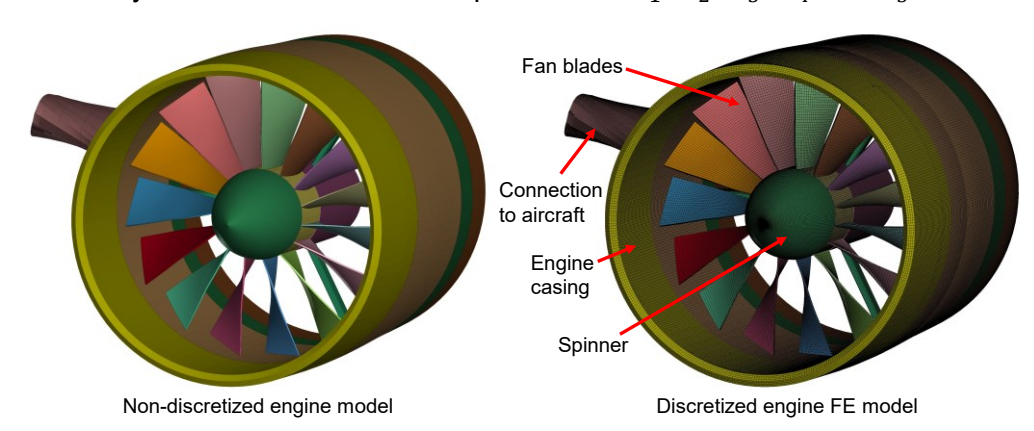


Figure 3 – Discretized engine model.

The lightweight and high-strength aerospace-grade aluminum alloy (AL 6061-T6) was selected as the material for the connection between the aircraft and engine casing as it is commonly used in structures of light aircraft and used in the FE model. The J-C material model was selected for the hard engine casing design and incorporated into the model using fully integrated shell elements. The reinforcement structure was also modeled internally to ensure structural stability. Other outer components of the engine model included the spinner, fan stage, exhaust cone, and three support struts connecting the engine to the aluminum casing. FOI into the engine typically results in damage to the fan blades and the casing for the most part [30] as the impactor gets disintegrated after colliding with the fan blades and casing. Therefore, to minimize the computational time for the simulations, the engine spinner, fan stage, exhaust cone, and support struts were assumed to be rigid bodies in the model with 304 stainless steel material properties and were modeled using fully integrated shell elements. The engine interior included a two-bearing system and a drive axle. These were also represented using the 304 stainless steel alloy, which has high strength and excellent corrosion resistance in high-temperature situations, making it suitable for applications in the aerospace. The interior components were modeled using fully integrated shell elements.

The relative motion of the hub was directly connected to the deformable axle as it undergoes comprehensive damage during the FOI. To retain the rotational motion, the drive axle was designed with a two-bearing system. Having a thrust bearing at the front and a ball bearing at the end of the axle helped restraining the translational motion of the assembly. Constraint-based tied contacts were used at the connection points for different components of the assembly. The tied constraint approach is well suited for connecting two parts with dissimilar mesh refinements [17, 30]. This is since elements do not need to be matched. It allows nodes of the follower component to be tied to the lead element based on proximity (offset option), hence enabling many nodes to be tied to a single element. The fan blades were connected to the fan stage hub using rigid constraints at their bases. The end nodes of connection to the aircraft and support struts were modeled as fixed rotational and translational boundaries, as shown in Fig. 4.

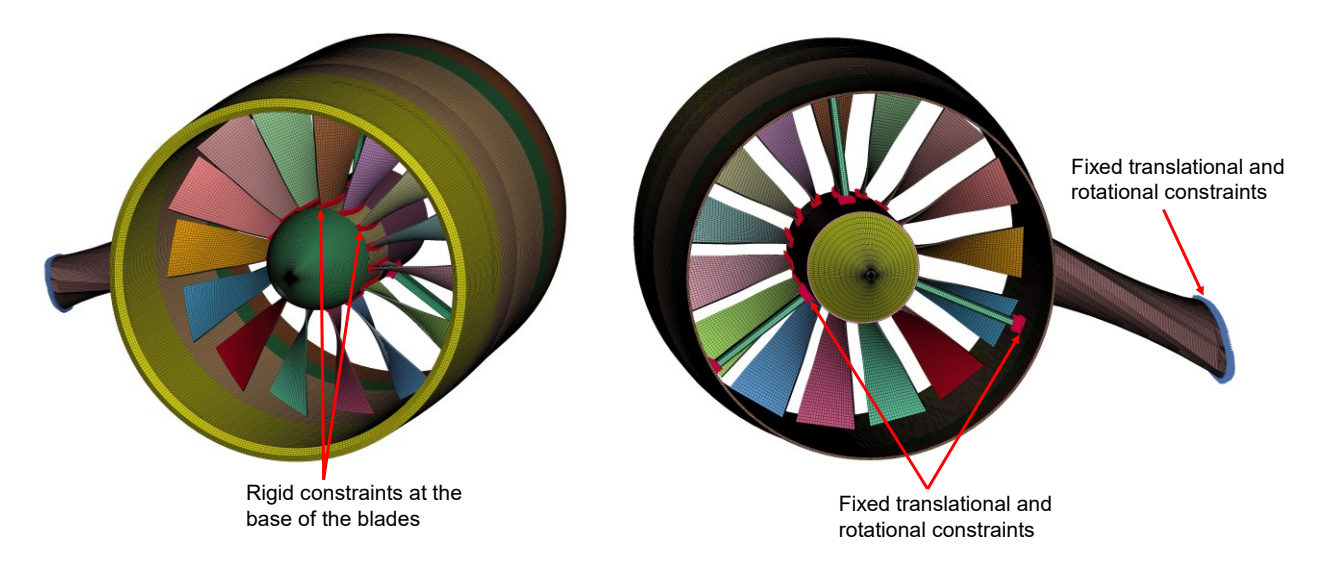


Figure 4 – Boundary constraints in engine model.

Centrifugal loads were present within every blade before the impact due to fan assembly rotation. Therefore, pre-loading of the fan blades was essential before activating the dynamic analysis [31]. Without dynamic relaxation, the instantaneous rotation can induce large unrealistic loads called centrifugal shocks in the blades before impact that can give rise to inaccurate impact-induced loads and forces. Therefore, dynamic relaxation (DR) was used to pre-stress the engine blades, where forces imposed on the blades by static or dynamically stable conditions were applied to the initially un-deformed blades. As the blades deform, nodal velocities were damped out at each time step [32] and tabulated. These nodal velocities and stresses were then applied as initial stresses and strains to the blades, resulting in pre-stressing of the blades before impact, simulating the engine in full motion. For the rotational motion of the assembly, the angular velocity was set to 500 rad/s, which is typical for similar type aircraft engines.

Upon impact, the blade that first came into contact with the projectile mass was subjected to high

crushing forces on the leading edge. The projectile material continued to flow over the blade and induced additional loads across its surface, in the direction opposite to the rotational direction. Any unbalance on the fan assembly due to impact can result in the blades located on the opposite side of the impact location to come into contact with the casing. This can produce large forces acting perpendicularly on the blade tip and down through the length of the blade, as well as shear loads on the blade tip [30]. Consequently, the contact of the blades with the casing can further result in normal and shear loads at the location of the contact between the blade tips and casing.

# 2.2 Impactor Models

Bird-strike on aircraft is classified as a soft-impact event. Soft impact occurs when the projectile has a much lower strength than the target, causing extensive deformation of the projectile [31, 33-41] over the target surface. Therefore, effective bird impact modeling requires to incorporate aspects of the theory of hydrodynamics. Based on this theory, upon impact, a shock is formed as a soft body comes into contact with a target. As the shock runs through the soft impactor in the opposite direction of the impact, it obliterates the internal bonds of the impactor and creates a release regime behind it and close to the impact side, where the soft matter having been transformed to a liquid bulk breaks from its original volumetric shape and disperses over the target. As the dispersion over the target at the point of impact and its vicinity continues, it produces a steady flow regime.

In this study, Smoothed Particle Hydrodynamics (SPH) technique is used to develop a representative FE bird model. The SPH soft body modeling approach requires the use of an equation of state (EOS) to represent the hydrodynamic pressure-volume relations in order to describe the high-pressure fronts created by the impactor. Several relevant equations have been used in past for bird impact studies [31, 43-49]. To simplify and streamline the analysis, water material properties can substitute the bird in the EOS. This follows by calibrating the EOS values until the peak pressure or impact pressure-time history profile observed approaches the experimental results reported by Wilbeck [38, 49]. In this study, a linear polynomial EOS was used based on Siddens et al. [30]

Following the current standard practices for the bird modeling approach, a cylindrical shape with hemispherical caps was considered to approximate the bird geometry. FAA 14 CFR § 23.2320(b) [7] requires the canopy of a Level 4 aircraft to withstand an impact without penetration from a 2 lb (900 g) bird. Considering this requirement, a bird mass of 900 g (2 lb) was modeled, constituting a large pigeon-size surrogate. Figure 5 shows the SPH bird model developed. A length-to-width ratio of 2 was chosen with a total number of particles of approximately 35,000. A density of 950 kg/m³ was used for the bird model, representative of water density with 10% air porosity.

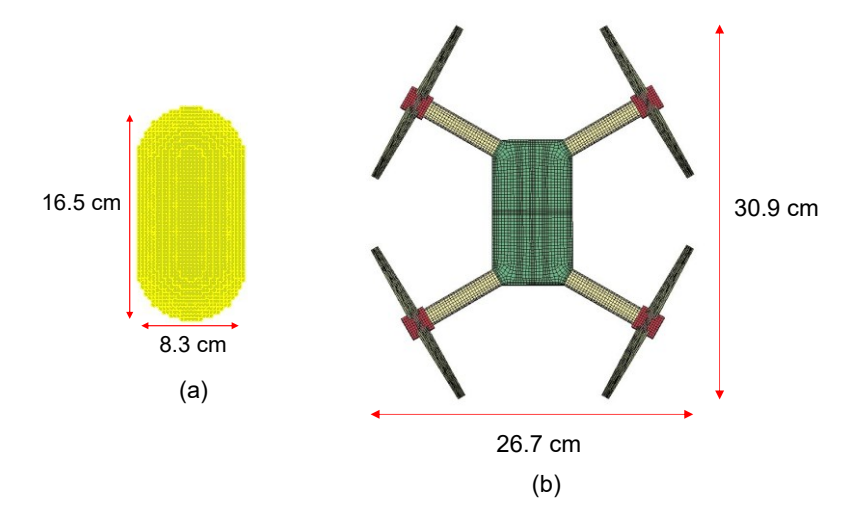


Figure 5 – (a) Cylindrical shape with hemispherical caps SPH bird impact model, (b) Quadcopter drone model used in this study.

The drone model was developed with a similar mass (900 g) to the bird model. As described above, birds are considered soft body objects with fluidic behavior during the impact. In contrast, drones have solid bodies that do not behave fluidic upon impact. Furthermore, during the impact, drones can break into smaller pieces with high density which can still cause further damage to other parts of the aircraft. Therefore, a drone impact scenario is considered a solid body impact. For this study, a quadcopter

drone was modeled with the main body, internal components, and propellers. The internal components included the battery, circuit board, motor, and other electronic components/circuit board. The battery was assigned lithium polymer (Li-Po) properties and was located inside the main body of the drone. Various electronic components with a range of material properties similar to circuit boards were included in the model and were assigned material properties of a glass-epoxy composite material [50]. The propellers were modeled using Nylon material properties and the main body, rotor hub, and arms were assumed to be made of acrylonitrile butadiene styrene (ABS). The motor was assumed to be made of aluminum alloy (AL 6061-T6). Elastic-plastic type material model was used to represent the material behaviors of the drone components [50] using fully integrated solid elements, except for the propellers which were represented using fully integrated shell elements.

# 2.3 Direct and Oblique Impact Locations

Direct and oblique impacts into the engine scenarios were modeled for both bird and drone impactors, as shown in Figs. 6 and 7. The target point was approximately 50% of the blade length for the direct impact scenarios based on the FAA regulations as per 14 CFR § 33.76(d)(3) [7], and approximately 75% of the blade length for the oblique impact scenarios. The velocity for the impact scenarios was determined to be 81 m/s, which corresponds to a combination of typical approach speeds of a small aircraft and a large pigeon. For consistency, drone impact was performed at the same velocity. The drone model was tilted forward by 25° based on the maximum tilt angle for similar-sized drones. The oblique impact scenarios for the bird and drone models considered the projectiles tilted diagonally at an angle of 45° from the line of direct impact and were moved upwards in the Z-direction to ensure impact occurs with blades and the casing primarily.

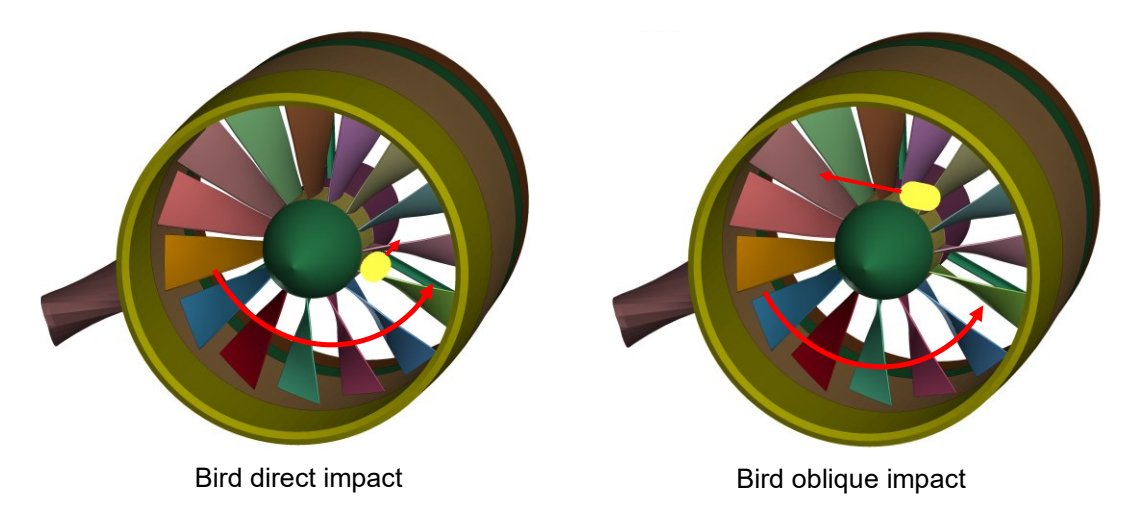


Figure 6 – Bird direct and oblique impact scenarios considered.

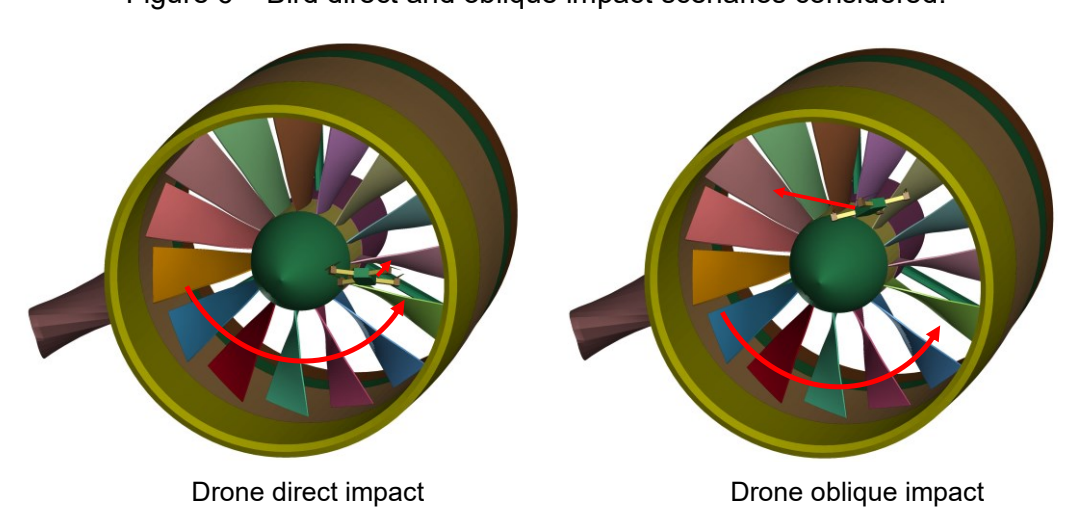


Figure 7 – Drone direct and oblique impact scenarios considered.

#### 3. Results and Discussion

The results of the bird and drone impact scenarios are presented in the form of von Mises stress as they provide a good overall behavior of the impacted structures, and plastic strain fringe plots in grayscale, highlighting the damage. Additionally, the impact force and energy-time history plots are also presented for each scenario and compared between the two impactors.

Stress and plastic strain results for the direct bird impact scenario are shown in Figs. 8 and 9. The impact sequence showed stress propagation as the impact progressed due to the bird model hitting and flying over the fan blade surfaces, while later getting sliced due to the fan rotation. The slicing of the bird model lead to a large SPH scatter due to particle acceleration, where kinetic energy from the fan rotation was transferred to the projectile mass. Stresses exceeding 300 MPa were recorded in the fan blades that come into direct contact with the bird. The resulting plastic strain in the impacted blades were found to be negligible as seen from the impact sequence in Fig. 9.

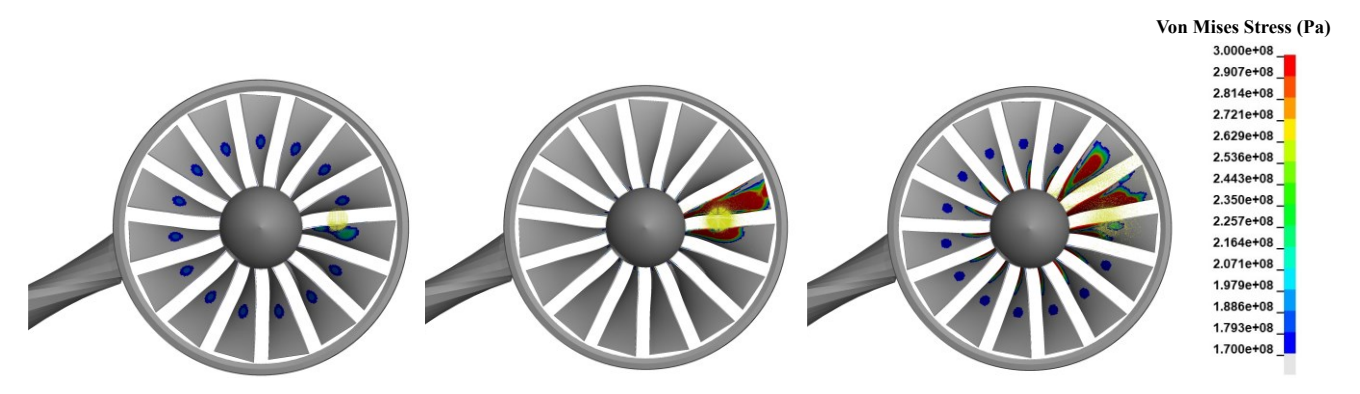


Figure 8 – Stress fringe plots for direct bird impact scenario.

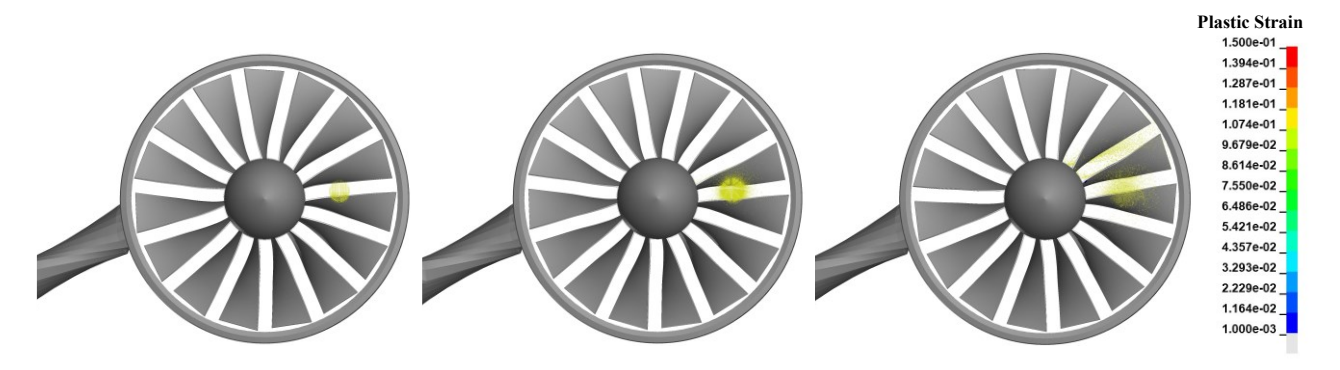


Figure 9 – Plastic strain fringe plots for direct bird impact scenario.

As the impact progressed, the fan blades continued to rotate. An unbalance in the rotation of the fan assembly was noted which lead to the fan blades coming into contact with the casing, resulting in sliding of the blades across the casing. This resulted in further damage in the form of permanent deformation in the casing as well as failure on the tip of the blades.

Stress and plastic strain results for the direct drone impact scenario are shown in Figs. 10 and 11. The impact sequence showed stress propagation as the drone went over the fan blade surfaces after the initial collision and was sliced by the rotating assembly. The collision of the drone model with the fan blades resulted in the drone breaking apart, which lead to the acceleration of drone debris due to the transfer of kinetic energy from the fan rotation to the projectile mass. Simulation results showed a large number of drone elements being deleted from the domain due to the activation of the erosion-based contact algorithm to limit large element deformations and avoid negative volume calculation. Due to drone element deletion, it is possible that the resulting drone debris in the simulations may not be inflicting as much damage as it could if the deleted drone element mass could be retained and hence could continue to collide with the engine. Stresses exceeding 300 MPa were recorded in the fan blades that came into direct contact with the drone. The resulting plastic strain in the impacted blades were found to be higher than the direct bird impact scenario. One of the impacted blade was noted to have extensive damage and failure due to its collision with the solid-body drone.

As the impact progressed and the fan blades continued to rotate, a slight unbalance in the rotation of the fan assembly was noted which lead to a number of fan blades in the opposite side of the impact coming into contact with the casing. This led to the sliding of the blades across the casing, resulting in further damage in terms of permanent deformation in the casing and failure of the blade tips. It is possible that if the deleted drone elements, and hence mass, could be preserved within the computational domain, they could continue to collide with the fan assembly and cause further unbalance and damage.

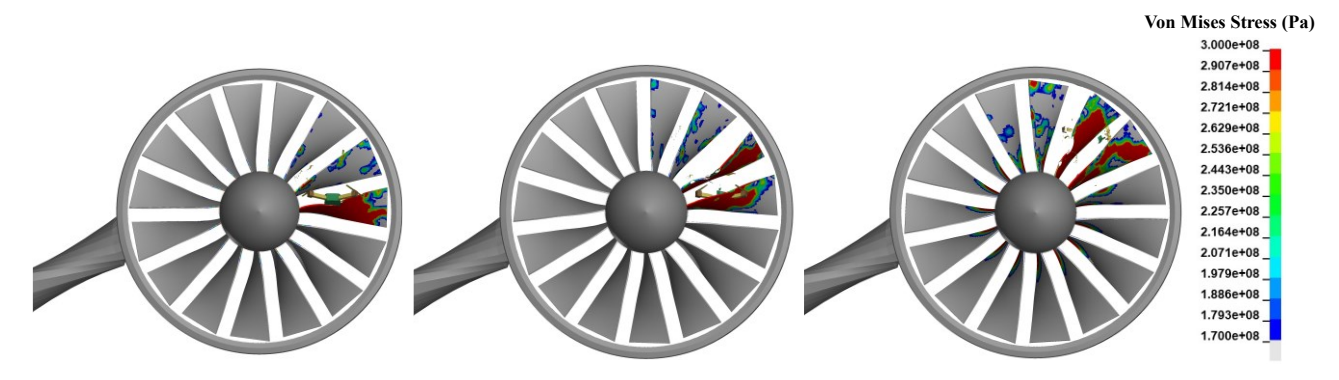


Figure 10 – Stress fringe plots for direct drone impact scenario.

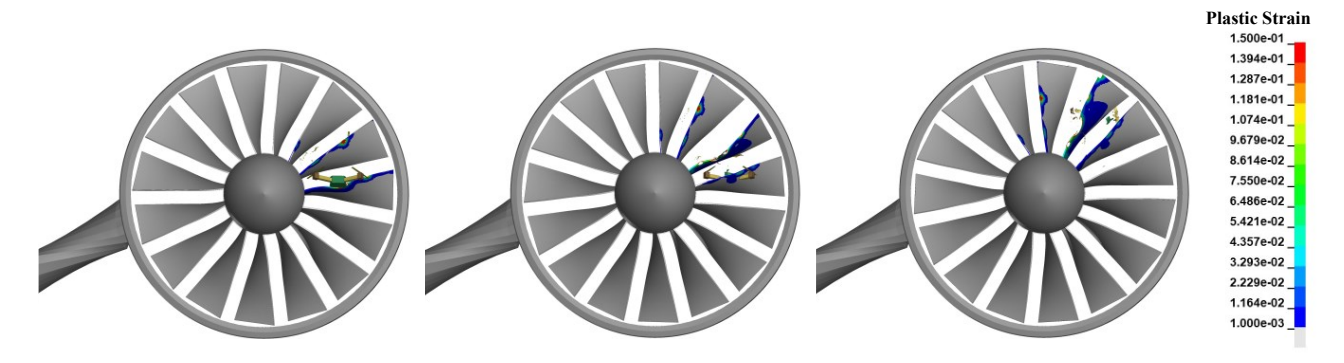


Figure 11 – Plastic strain fringe plots for direct drone impact scenario.

Stress and plastic strain results for the oblique bird impact scenario are shown in Figs. 12 and 13. The impact results showed stress propagation as the bird model collided with the fan blades and slid over the blade surfaces. The slicing of the bird model due to fan rotation lead to a large scatter of the SPH particles near the blade tips against the casing. Stresses exceeding 300 MPa were recorded in the fan blades that came into direct contact with the bird model. The resulting plastic strain in the impacted blades were found to be mostly at the blade tips as seen from the impact sequence in Fig. 13.

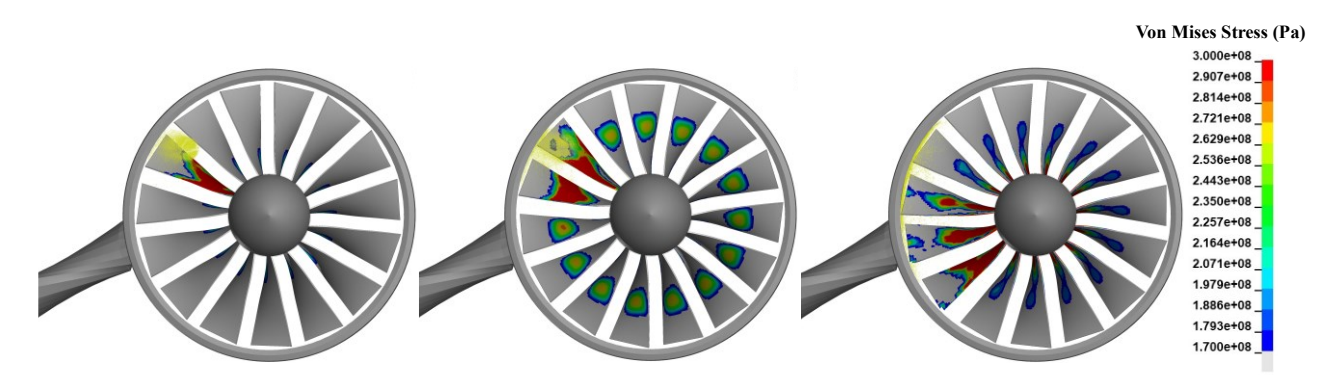


Figure 12 – Stress fringe plots for oblique bird impact scenario.

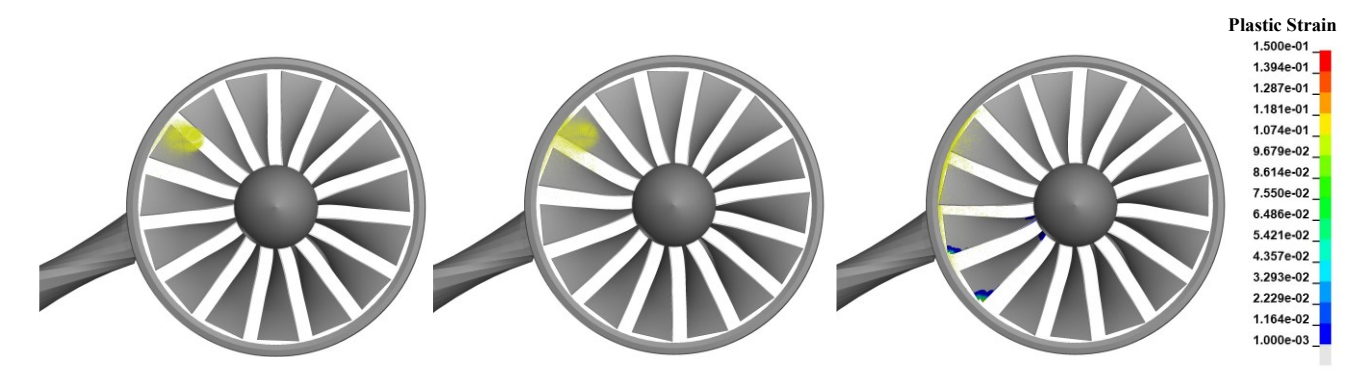


Figure 13 – Plastic strain fringe plots for oblique bird impact scenario.

As the impact progressed, rotational unbalance was noted which led to the fan blades coming into contact with the casing. This led to the sliding of the blades across the casing. Due to the bird SPH particles being scattered near the blade tips and the casing after the initial impact, more permanent deformation in the casing and blade tips was observed, when compared to the direct impact scenario. Stress and plastic strain results for the direct drone impact scenario are shown in Figs. 14 and 15. The impact results showed stress propagation as the drone further collided with the fan blades and their surfaces, while the fan assembly was rotating. The collision with the fan blades resulted in the drone breaking apart, with its fragments accelerated within the engine cavity due to the high kinetic energy transferred from the rotating fan assembly. The majority of the drone debris was noted to collide with the casing. Stresses in the fan blades that came directly into contact with the drone were found to be much higher than in the oblique bird impact scenario. The resulting plastic strain in the impacted blades were also found to be higher than the oblique bird impact scenario. One of the impacted blades was noted to have extensive damage and failure due to its collision with the solid-body drone, similar to the direct drone impact scenario.

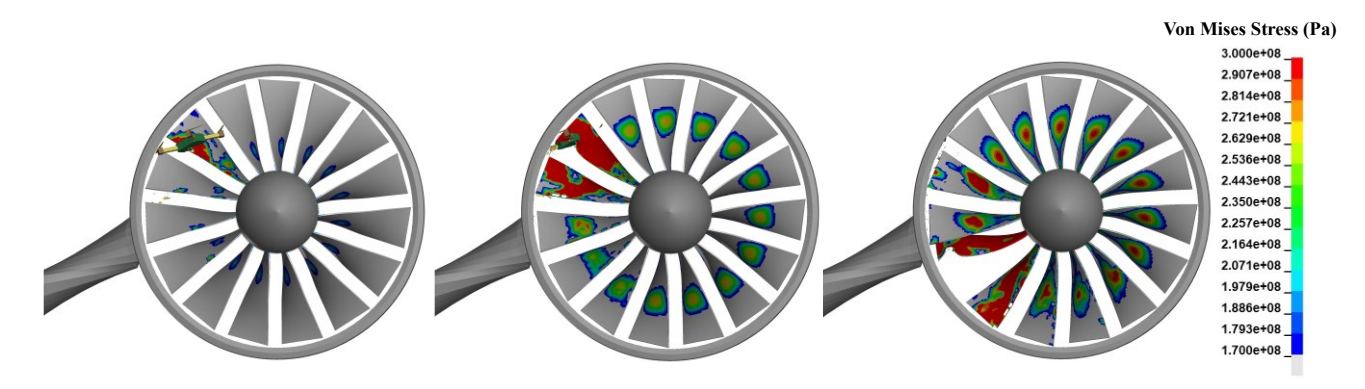


Figure 14 – Stress fringe plots for oblique drone impact scenario.

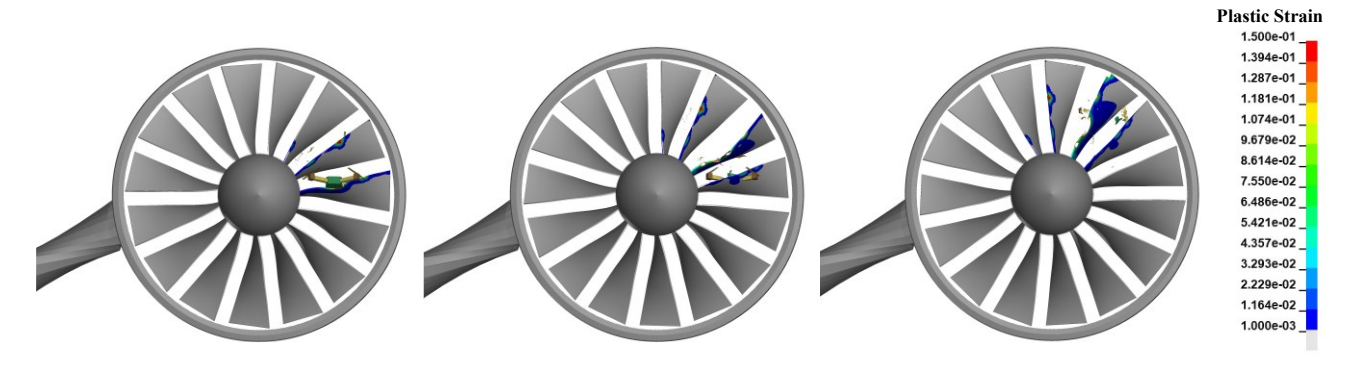


Figure 15 – Plastic strain fringe plots for oblique drone impact scenario.

As the impact progressed and the fan blades continued to rotate, an unbalance in the rotation of the fan assembly was noted which lead to the fan blades in the opposite side of the impact region coming into contact with the casing. This lead to the sliding of the blades across the casing resulting in permanent deformation in the casing as well as failure in the blade tips. It is possible that if the deleted

drone element mass was preserved, further damage to the casing and blades could have ensued. The impact force-time histories are plotted and compared between the direct and oblique impact scenarios for the bird and drone in Figs. 16 and 17. Impact force results are provided for the first four individual fan blades that came into contact with the projectile. For the direct impact scenario, the highest impact force was recorded on the second blade that came into contact with the bird SPH model, registering approximately 24 kN, whereas for the drone case, it was also the second blade that came into contact with the drone model, however registering a peak force of nearly 120 kN. Subsequently, the impact with the third blade also resulted in a much higher peak force for the drone model (80 kN) when compared to the bird model (12.5 kN).

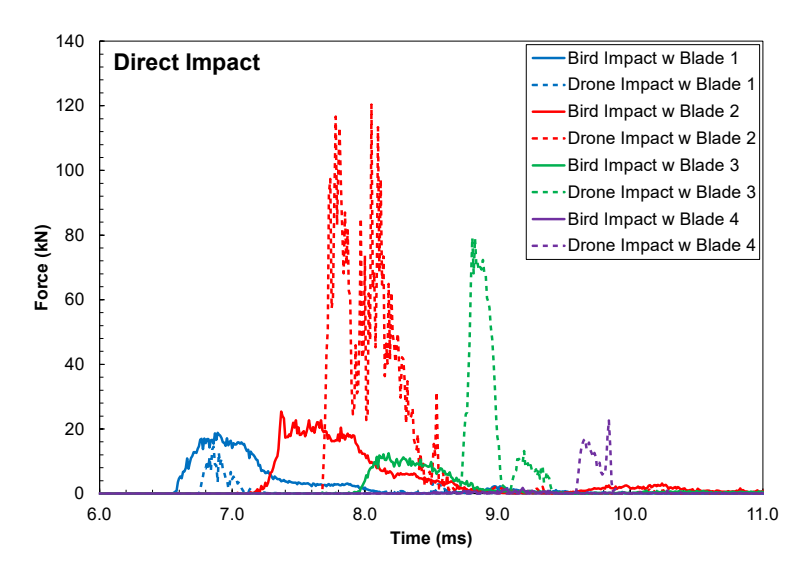


Figure 16 – Impact force comparison between bird and drone cases for direct impact scenarios.

For the oblique impact scenario, the highest impact force was recorded on the second blade that came into contact with the bird SPH model, registering approximately 28.6 kN, whereas for the drone case, it was the third blade that came into contact with the drone model, registering a peak force of around 200 kN. This highlights a substantial difference in the impact force between the bird and the drone models, underlining the severity and criticality of the impact of the fan blades with a solid body as compared to a soft body.

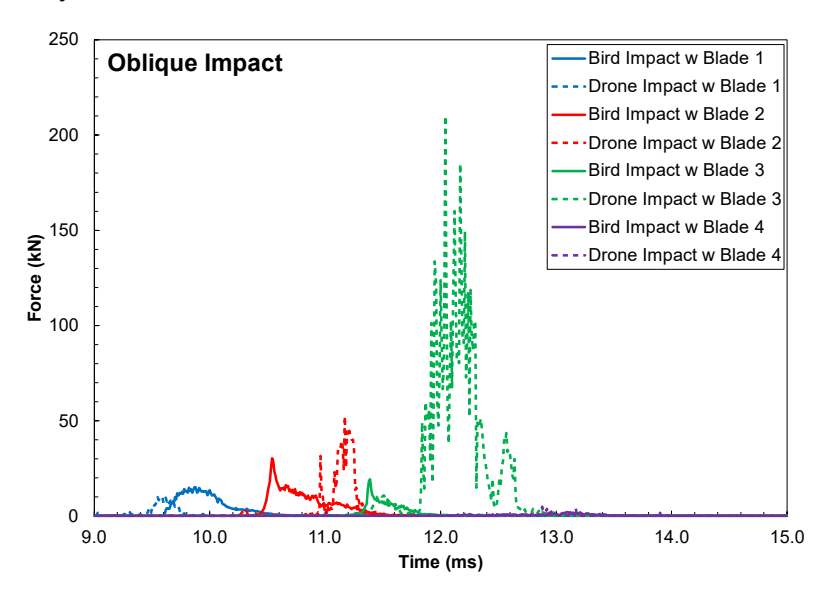


Figure 17 – Impact force comparison between bird and drone cases for oblique impact scenarios.

The results shown are without any data filtering, therefore it is possible that the instantaneous peak force magnitudes could be reduced after applying any filtering schemes. However, the conclusion based on these results would remain the same, that a drone impact leads to higher impact forces on the aircraft engine blades as opposed to a bird-strike.

The energy-time histories for the direct and oblique impact scenarios are shown in Figs. 18 and 19 for

both bird and drone impacts. The results show the internal, kinetic and total energy of the impacted system. The hourglass energies were found to be zero due to the use of fully integrated elements in the simulations. The kinetic energy of the impacted system fluctuated around its initial value of 500 kJ due to the continuous rotational motion of the fan assembly throughout the impact window. This energy was noted to decrease as the impact progressed, which is expected as a portion of the fan blades kinetic energy was transferred to the projectiles during impact.

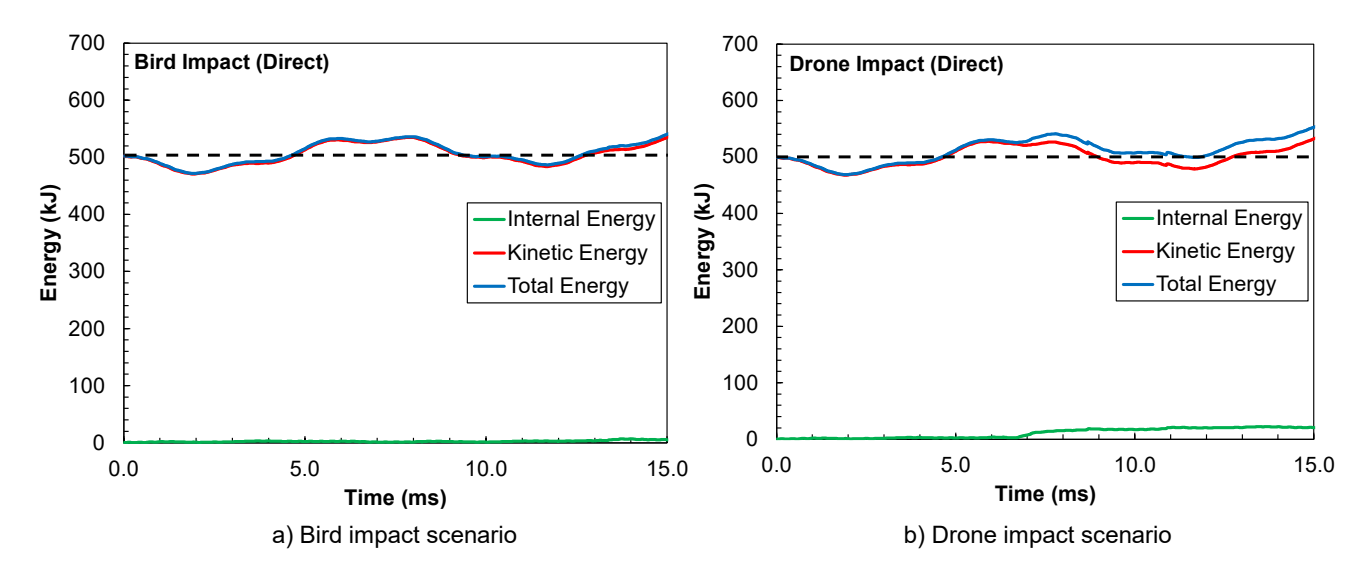


Figure 18 – Energy-time histories for direct impact scenarios for bird and drone models.

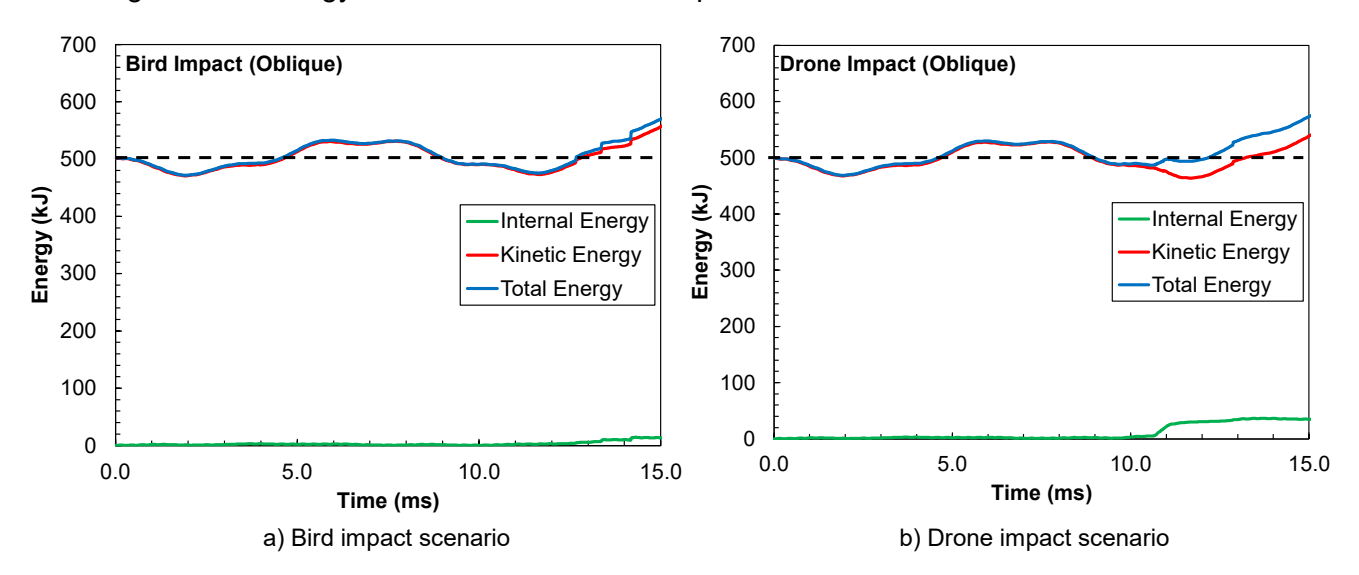


Figure 19 – Energy-time histories for oblique impact scenarios for bird and drone models.

In contrast, the internal energy of the system increased as the impact progressed. As the contact took place between the projectiles and the system, the projectile slowed down due to the collision, which in turn reduced its initial kinetic energy. This energy was transferred to the impacted system where it was converted into internal energy, thereby resulting in an increase in the system's internal energy.

#### 4. Conclusion

Direct and oblique impacts using SPH bird surrogate and quadcopter drone FE model with a similar mass of 900 g, were simulated on a modern ODAM aircraft engine powered using an electric powertrain. The projectiles were targeted primarily at the fan blades at approximately 50% of the blade length for the direct impact scenarios and 75% of the blade length for the oblique impact scenarios, as well as the casing. The resultant impact forces, stresses strain, and energies were output and reported. For the impact cases considered as part of this crashworthiness study, the drone model produced higher peak forces in both direct and oblique impact scenarios. The impact forces resulting from the drone collision on the fan blades were significantly higher than those of the bird's. The drone in both direct and oblique impact scenarios resulted in permanent deformation of the leading edge

and blade tip for multiple blades, and blade failure for one of the blades due to significant structural damage. The bird in both direct and oblique impact scenarios produced a similar magnitude of stresses in the blade as the drone, however, did not result in severe blade damage. In the bird scenarios, only some permanent deformation was noted, mostly at the blade tip.

The stress distribution overall was found to be similar for both the bird and drone for direct impact scenarios, however, higher stresses were noted in the fan blades for the oblique impact case for the drone. In terms of damage to the fan blades, oblique impacts from the bird and drone models provided more adverse results as compared to direct impacts. In terms of casing damage, oblique impacts resulted in more direct contact between the projectiles leading to further unbalanced in rotation. The unbalance in turn caused the blades to slide across the casing, creating added permanent deformation for the casing and blade tips. When compared to the direct impact scenarios, it was observed that a lower level of unbalance in the fan assembly produced less permanent deformation at the blade tip and casing.

The drone impact scenarios in this study had incorporated an erosion-based contact algorithm to ensure simulation stability. However, including this algorithm enabled element and, thereby, mass deletion from the computational domain after the initial impact. In contrast, the SPH bird model particles scattered across the fan blades and casing after the impact as no SPH particles were deleted. In real-life scenarios, after fragmentation, the drone pieces and debris can also create a scatter cloud hitting internal engine components, hence causing further damage to the engine than what is determined in this study. Nonetheless, considering the overall results of the analyses presented, it is shown that ingested drones with high stiffness components can cause critical damage to the conventional fan assemblies, as opposed to comparable soft bodies, based on which contemporary engine crashworthiness characteristics and airworthiness regulations have been developed and founded, respectively. Therefore, for the same mass category and based on a series of high-fidelity simulations, it is evident that impact of drones with high stiffness parts can lead to more consequential engine damage. To ensure safety, future propulsion research and development programs will be required to carefully consider this foreign object ingestion threat, be it from the design-, or air-traffic management perspective (or both).

## 5. Contact Author Email Address

Corresponding author:

Javid Bayandor; bayandor@buffalo.edu

## 6. Copyright Statement

The authors confirm that they, and/or their company or organization, hold copyright on all of the original material included in this paper. The authors also confirm that they have obtained permission, from the copyright holder of any third party material included in this paper, to publish it as part of their paper. The authors confirm that they give permission, or have obtained permission from the copyright holder of this paper, for the publication and distribution of this paper as part of the ICAS proceedings or as individual off-prints from the proceedings.

### References

- [1] Johnson W. and Silva C. NASA concept vehicles and the engineering of advanced air mobility aircraft. *The Aeronautical Journal*, vol. 126, no. 1295, pp. 59-91, 2021, doi: <a href="https://doi.org/10.1017/aer.2021.92">https://doi.org/10.1017/aer.2021.92</a>.
- [2] Schuh G., Spangenberg M., and Freitag M. Assessment of Top Level Specifications for Urban and Regional Air Mobility Vehicles. Deutsche Gesellschaft für Luft- und Raumfahrt Lilienthal-Oberth e.V. (Text), 2021, doi: https://doi.org/10.25967/530312.
- [3] Vaghela P., Raza H., Stumpf E., and Bayandor J. High Fidelity Airworthiness Bird and Drone Strike Analysis of On-Demand Air Mobility Service Aircraft. in *33rd Congress of the International Council of the Aeronautical Sciences*, Stockholm, Sweden, 2022.
- [4] Stumpf E., Kreimeier M., Strathoff P., Lückhof J., Schröder K. U., and Janser F. Small aircraft concept for regional on-demand air mobility. in *31st Congress of the International Council of the Aeronatutical Sciences*, Belo Horizonte, Brazil, 2018.
- [5] Wright S. E. and Dolbeer R. A., "Some Significant Wildlife Strikes To Civil Aircraft In The Unit The United States, January 2005 March 2006," presented at the USDA National Wildlife Research Center Staff Publications. 135, 2006. [Online]. Available: https://digitalcommons.unl.edu/icwdm\_usdanwrc/135

- [6] Richard A., and Dobleer M. J. B., "Wildlife Strikes to Civil Aircraft in the United States, 1990 2019," in *National Wildlife Strike Database*, ed: Federal Aviation Administration, 2019.
- [7] Part 23 Airworthiness Standards: Normal Category Airplanes, FAA, 2021.
- [8] Xianghao M. *et al.* Dynamic response of the horizontal stabilizer during UAS airborne collision. *International Journal of Impact Engineering*, vol. 126, pp. 50-61, 2019.
- [9] Ruchti J., Senkbeil R., Carroll J., Dickinson J., Holt J., and Biaz S. Unmanned Aerial System Collision Avoidance Using Artificial Potential Fields. *Journal of Aerospace Information Systems*, vol. 11, no. 3, pp. 140-144, 2014.
- [10] Yasin J. N., Mohamed S. A. S., Haghbayan M.-H., Heikkonen J., Tenhunen H., and Plosila J. Unmanned Aerial Vehicles (UAVs): Collision Avoidance Systems and Approaches. *Institute of Electrical and Electronics Engineers Access*, vol. 8, pp. 105139-105155, 2020.
- [11] Schroeder K., Song Y., Horton B., and Bayandor J., "Investigation of UAS Ingestion into High-Bypass Engines, Part 2: Parametric Drone Study," presented at the 58<sup>th</sup> AIAA/ASCE/AHS/ASC Structures, Structural Dynamics, and Materials Conference, Grapevine, Texas, 2017.
- [12] Song Y., Horton B., and Bayandor J., "Investigation of UAS ingestion into high-bypass engines, Part 1: Bird vs. Drone," presented at the 58<sup>th</sup> AIAA/ASCE/AHS/ASC Structures, Structural Dynamics, and Materials Conference, Grapevine, Texas, 2017.
- [13] Megharaja S. J. and Bayandor J. Comprehensive Analysis of Fluid-Structure Interactive Schemes for Modeling Aircraft Water Impact Scenarios. in *ASME 2020 Fluids Engineering Division Summer Meeting*, 2020: American Society of Mechanical Engineers.
- [14] Siddens A. J., Bayandor J., and Abdi F. Soft impact damage prognosis of F-16 canopy using progressive failure dynamic analysis. *Journal of Aircraft*, vol. 51, no. 6, pp. 1959-1965, 2014.
- [15] Dobleer R. A. Height Distribution of Birds Recorded by Collisions with Civil Aircraft. *USDA National Wildlife Research Center*, 2006.
- [16] Nicholson R. and Reed W. S. Strategies for Prevention of Bird-strike Events. *Boeing AERO Magazine*, vol. QTR\_03, pp. 17-24, 2011. [Online]. Available: <a href="https://www.boeing.com/commercial/aeromagazine/articles/2011\_q3/pdfs/AERO\_2011\_Q3.pdf">https://www.boeing.com/commercial/aeromagazine/articles/2011\_q3/pdfs/AERO\_2011\_Q3.pdf</a>.
- [17] Song Y., "Development of Comprehensive Dynamic Damage Assessment Methodology for High-Bypass Air Breathing Propulsion Subject to Foreign Object Ingestion," ed, 2016.
- [18] Hasan Raza (incorrect format) O. R. G., Kevin Carpenter, Tuomas Pärnänen, Jarno Jokinen, Mikko Kanerva, Javid Bayandor. Predictive methods for initiation of delamination and intralaminar damage in carbon fibre reinforced polymer laminates subject to impact. *The Aeronautical Journal*, vol. 128, no. 1323, pp. 846-874, 2023, doi: https://doi.org/10.1017/aer.2023.95.
- [19] Raza H., Harley C., Vaghela P., and Bayandor J. Development of a Predictive Damage Methodology for Hybrid Wing Body Aircraft Structures. in *Proceedings of 33<sup>rd</sup> International Congress of Aeronautical Sceineces*, Stockholm, Sweden, 4-9 September 2022: International Council of Aeronautical Sciences.
- [20] LSTC, "LS-Dyna: Keyword Users Manual Volume 1," ed: ANSYS (previously Livermore Software Technology Corporation), 2021, p. 3826.
- [21] Shivpuri R., Hua J., Mittal P., Srivastava A., and Lahoti G. Microstructure-mechanics interactions in modeling chip segmentation during titanium machining. *CIRP Annals*, vol. 51, no. 1, pp. 71-74, 2002.
- [22] Meyer Jr H. W. and Kleponis D. S. Modeling the high strain rate behavior of titanium undergoing ballistic impact and penetration. *International Journal of Impact Engineering*, vol. 26, no. 1-10, pp. 509-521, 2001.
- [23] Lee W.-S. and Lin C.-F. Plastic deformation and fracture behaviour of Ti–6Al–4V alloy loaded with high strain rate under various temperatures. *Materials Science and Engineering: A,* vol. 241, no. 1-2, pp. 48-59, 1998.
- [24] Lee W.-S. and Lin C.-F. High-temperature deformation behaviour of Ti6Al4V alloy evaluated by high strain-rate compression tests. *Journal of Materials Processing Technology*, vol. 75, no. 1-3, pp. 127-136, 1998.
- [25] Wang C., Suo T., Li Y., Xue P., and Tang Z. A new experimental and numerical framework for determining of revised JC failure parameters. *Metals*, vol. 8, no. 6, p. 396, 2018.
- [26] Milani A., Dabboussi W., Nemes J. A., and Abeyaratne R. An improved multi-objective identification of Johnson–Cook material parameters. *International journal of impact engineering*, vol. 36, no. 2, pp. 294-302, 2009.

- [27] Yatnalkar R. S., "Experimental investigation of plastic deformation of Ti-6Al-4V under various loading conditions," The Ohio state university, 2010.
- [28] Hammer J. T., "Plastic deformation and ductile fracture of Ti-6Al-4V under various loading conditions," The Ohio State University, 2012.
- [29] Lesuer D. R., "Experimental Investigations of Material Models for Ti-6a1-4v Titanium and 2024-T3 Aluminum," 2000.
- [30] Siddens A. J., "A Predictive Methodology for Soft Impact Damage in Jet Engines Incorporating Hybrid Composite Structures," Master's Thesis, Virginia Polytechnic Institue, Blacksburg, VA, 2012.
- [31] Siddens A. and Bayandor J., "Multidisciplinary impact damage prognosis methodology for hybrid structural propulsion systems," in *Computers and Structures* vol. 122, ed: Elsevier Ltd, 2013, pp. 178-191.
- [32] LSTC, "LS-Dyna Theory Manual," ed: ANSYS (previously Livermore Software Technology Corporation), 2019.
- [33] Siddens A. and Bayandor J., "An extensive crashworthiness methodology for advanced propulsion systems, Part II: Damage and vibration instability analysis of jet engine forward sections," in 49th AIAA Aerospace Sciences Meeting Including the New Horizons Forum and Aerospace Exposition, ed, 2011, pp. 1-11.
- [34] Kim M., Zammit A., Siddens A., and Bayandor J., "An Extensive crashworthiness methodology for advanced propulsion systems, Part I: Soft impact damage assessment of composite fan stage assemblies," in 49th AIAA Aerospace Sciences Meeting Including the New Horizons Forum and Aerospace Exposition, ed, 2011, pp. 1-16.
- [35] Zammit A., Kim M., and Bayandor J. Bird-strike damage tolerance analysis of composite turbofan engines. in *27th congress of the international council of the aeronautical sciences*, 2010, vol. 4, pp. 2824-2840.
- [36] Bayandor J., Johnson A., Thomson R. S., and Joosten M. Impact damage modelling of composite aerospace structures subject to bird-strike. in *25th International congress of the aeronautical sciences*, 2006.
- [37] Joosten M. and Bayandor J. Coupled SPH-composite cohesive damage modeling methodology for analysis of solid-fluid interaction. in *46th AIAA Aerospace Sciences Meeting and Exhibit*, 2008, p. 1424.
- [38] Wilbeck J. S. and Rand J. L. The development of a substitute bird model. *Journal of Engineering for Gas Turbines and Power,* vol. 103, no. 4, pp. 725-730, 1981.
- [39] Ritt S. A. and Oswald J., "Analysis of Hard and Soft Body Impact on Rotorcraft Windshields," presented at the Aerospace Structural Impact Dynamics International Conference, 2019.
- [40] Pernas-Sánchez J., Artero-Guerrero J., Varas D., and López-Puente J., "Validation and analysis of bird substitute impact on Hopkinson tube," presented at the Aerospace Structural Impact Dynamics International Conference, 2019.
- [41] Song Y., Bayandor J., and Horton B., "A Contribution to Full-Scale High Fidelity Aircraft Progressive Dynamic Damage Modeling for Certification by Analysis," presented at the Aerospace Stuctural Impact Dynamics International Conference, 2015.
- [42] Jenq S.-T., Hsiao F.-B., Lin I., Zimcik D., and Ensan M. N. Simulation of a rigid plate hit by a cylindrical hemi-spherical tip-ended soft impactor. *Computational materials science*, vol. 39, no. 3, pp. 518-526, 2007.
- [43] Vignjevic R., Orłowski M., De Vuyst T., and Campbell J. C., "A parametric study of bird-strike on engine blades," in *International Journal of Impact Engineering* vol. 60, ed, 2013, pp. 44-57.
- [44] Moffat T. J. and Cleghorn W. L., "Prediction of bird impact pressures and damage using MSC/DYTRAN," in *Proceedings of the ASME Turbo Expo* vol. 4, ed, 2001, pp. 1-9.
- [45] McCarthy M. A. *et al.*, "Modelling of bird-strike on an aircraft wing leading edge made from fibre metal laminates Part 2: Modelling of impact with SPH bird model," in *Applied Composite Materials* vol. 11, ed, 2004, pp. 317-340.
- [46] Liu J., Li Y., and Gao X., "Bird-strike on a flat plate: Experiments and numerical simulations," in *International Journal of Impact Engineering* vol. 70, ed: Elsevier Ltd, 2014, pp. 21-37.
- [47] Lavoie M. A., Gakwaya A., Ensan M. N., Zimcik D. G., and Nandlall D., "Bird's substitute tests results and evaluation of available numerical methods," in *International Journal of Impact Engineering* vol. 36, ed: Elsevier Ltd, 2009, pp. 1276-1287.
- [48] Allaeys F., Luyckx G., Van Paepegem W., and Degrieck J., "Numerical and experimental investigation of the shock and steady state pressures in the bird material during bird-strike," in

- International Journal of Impact Engineering vol. 107, ed: Elsevier Ltd, 2017, pp. 12-22.
- [49] Wilbeck J. S., "Impact Behaviour of Low Strength Projectile," Air Force Materials Laboratory, 1977.
- [50] Liu H., Che Man M. H., and Low K. H. UAV airborne collision to manned aircraft engine: Damage of fan blades and resultant thrust loss. *Aerospace Science and Technology*, vol. 113, 2021, doi: <a href="https://doi.org/10.1016/j.ast.2021.106645">https://doi.org/10.1016/j.ast.2021.106645</a>.
- [51] Nizampatnam L. S., "Models and Methods for Bird-strike Load Predictions," Ph.D. Dissertation, Dept. of Aerospace Engineering, Wichita State University, Wichita, KS, 2007.